ÉCOLE POLYTECHNIQUE

Thèse présentée pour obtenir le grade de

DOCTEUR DE L'ECOLE POLYTECHNIQUE

Spécialité : Mécanique

par

Anne-Virginie SALSAC

EVOLUTION DES CONTRAINTES HEMODYNAMIQUES LORS DE LA CROISSANCE DES ANEVRISMES AORTIQUES ABDOMINAUX

Thèse soutenue le 7 février 2005 devant le jury composé de :

J. M. Chomaz	Directeur de thèse
J. C. Lasheras	Co-directeur de thèse
D. Barthès Biesel	Examinateur
P. F. Linden	Rapporteur
C. Legallais	Rapporteur

The dissertation of Anne-Virginie Salsac is approved, and it is acceptable in quality and form for publication on microfilm:

_____

_____

_____

_____

_____

_____

Co-chair

_____

Chair

University of California, San Diego

2005

Table of Contents

Signature Page iii

Table of Contents iv

List of Symbols vii

List of Figures xi

Acknowledgements xvii

Vita xix

Abstract xxi

I. General introduction 1

A. Changes in the wall composition involved in the formation, enlargement and rupture of the disease 4

B. Pathogenesis of abdominal aortic aneurysms 9

C. Influence of the hemodynamic forces on the pathology 11

1. Endothelial cells 11

2. Smooth muscle cells 14

3. Platelets 14

D. Changes in the hemodynamics in abdominal aortic aneurysms 17

E. Objectives of the study 19

F. Structure of the thesis 20

II. Methods 21

A. Experimental apparatus 21

1. Aneurysm models 21

2. Experimental setup 24

B. Particle Image Velocimetry 27

III. Evolution of the wall shear stresses during the progressive enlargement of symmetric abdominal aortic aneurysms....29
A. Introduction....29
B. Experimental setup....31
C. Characteristics of the flow in a healthy abdominal aorta....31
1. Measurements of the flow in a healthy abdominal aorta....31
2. Analytical solution of the flow in a healthy abdominal aorta....35
D. Flow in abdominal aortic aneurysms....39
1. Results of the parametric study of the flow characteristics in AAAs..39
2. Results of the parametric study of the wall shear stresses in AAAs....52
3. Analytical solution for a slowly expanding abdominal aorta....62
E. Discussion....67
F. Conclusion....72
IV. Effects of the loss of symmetry on the wall shear stresses in abdominal aortic aneurysms....75
A. Introduction....75
B. Experimental setup....76
C. Results....76
1. Flow characteristics in abdominal aortic aneurysms....76
2. Patterns of WSS and GWSS in AAAs....88
3. Extension to anatomically correct geometries....96
D. Discussion....98
E. Conclusion....101
V. Physiological relevance of the changes in the hemodynamics for circulating blood cells in Abdominal Aortic Aneurysms....103
A. Introduction....103

B. Material and methods 104
C. Results 108
1. Influence of the AAA on the cell trajectories, residence time and stress history 108
2. Effects of the aspect ratio 112
3. Effects of the dilatation ratio 114
4. Effects of the asymmetry parameter 117
D. Discussion 120
E. Conclusion 124
VI. General conclusion and perspectives 127
A. General conclusion 127
B. Perspectives 131
Appendix A 135
A. Calculation of the strain rates 135
B. Calculation of the vorticity and stress fields 136
C. Calculation of the wall shear stresses 137
Appendix B 139
Appendix C 141
References 143

LIST OF SYMBOLS

A	Activation field
a	Inner local radius
a_0	Inner radius of the parent vessel ($a_0 = d/2$)
d	Inner diameter of the parent vessel
D	Maximum inner diameter of the aneurysm
e	Eccentricity of the aneurysm bulge
f	Frequency of the flow waveform
F	Non-dimensionalized variable of α_n
G_n	Pressure Fourier coefficient
h	Distance of the blood cell to the wall
i	Complex number or grid position in the x-direction
j	Grid position in the y-direction
J_n	Bessel function of the first kind of order n
l	Maximum length traveled by the vortex ring inside the aneurysm
L	Aneurysm length
n	Order of the mode in the Fourier decomposition
$\vec{n}$	Normal unit vector
p	Pressure
P	New pressure such that $P^* = \varepsilon\, p^*$.
R	Non-dimensionalized local radius in aneurysm
Q	Flow rate
r	Space variable in the radial direction
Re	Reynolds number
St	Strouhal number

St_{syst}	Strouhal number calculated with the systolic time t_{syst}
t	Time variable
$\vec{t}$	Tangential unit vector
T	Period of the flow waveform
t_0	Time of release of a blood cell at the entrance of an aneurysm
t_1	Time a blood cell exits the aneurysm
U	Characteristic velocity
u	x-component of the velocity vector
u_r	r-component of the velocity vector
U_r	New radial velocity such that $u_r^* = \varepsilon U_r^*$
v	y-component of the velocity vector
x	Space variable in the perpendicular direction to the flow
y	Space variable in the direction of the flow
Y	New space variable in the y-direction such that $Y^* = \varepsilon y^*$

Greek symbols

α	Womersley number
α_n	Womersley number based on the n^{th} Fourier model
β	Asymmetry parameter
Δx	distance traveled by the cell in the x-direction between 2 time steps
Δy	distance traveled by the cell in the y-direction between 2 time steps
ε	Small parameter $\varepsilon = \Lambda / a_0$
Λ	Characteristic length along which the local radius a changes
μ	Dynamic viscosity
ν	Kinematic viscosity

ρ	Density
σ	Rate of deformation tensor for a Newtonian fluid
Σ	Relaxation time-scale of the shear stresses on cells
τ	Local total stress
$\tau_{1, 2, 3}$	3 eigenvalues of the rate of deformation tensor σ
$\tau_{mean,H}$	Mean total stress measured in the healthy parent vessel
ω	Pulsation of the flow
ω_z	z-component of the vorticity vector

Conventions

X^*	Non-dimensionalized form of X
X_p	Peak value of X
$\overline{X}$	Time-average of X
$\langle X \rangle$	Space-average of X
∇	Gradient

Frequently used acronyms

AAA	Abdominal aortic aneurysm
CAF	Cell activation factor
EC	Endothelial cells
GWSS	Gradient of wall shear stresses
ILT	Intraluminal thrombus
LDL	Low density lipoprotein
MRI	Magnetic resonance imaging

NWRT	Near wall residence time
OSI	Oscillatory shear index
PIV	Particle image velocimetry
WSS	Wall shear stresses
WSS_{mean}	Time-average of the wall shear stresses
WSS_{mag}	Magnitude of the wall shear stresses

LIST OF FIGURES

Figure 1.1: Abdominal aortic aneurysm 2

Figure 1.2: (*a*) Anatomy of the abdominal trunk, (*b*) Abdominal aortic aneurysm 2

Figure 1.3: Spiral computed tomography (CT) with 3-D reconstruction showing an abdominal aneurysm originating below the renal arteries 3

Figure 1.4: Wall composition of an arterial wall (Johansen 1982)..... 5

Figure 1.5: Elastic diagram of normal and aneurysmal aortic walls. Shift of the curves corresponding to aneurysmal walls compared to the curves for normal vessels. 7

Figure 1.6: CT scan through an 8.5 cm AAA. The thrombus has filled most of the aneurysm, leaving a lumen with a diameter close to the size in a healthy vessel..... 8

Figure 1.7: Morphology of endothelial cells (*a*) before and (*b*) after applying shear stress (M. Sato) 13

Figure 2.1: Sketches of a small ($D < 4.5$ cm) and later stage aneurysm..... 22

Figure 2.2: Geometry of a symmetric aneurysm model. 22

Figure 2.3: Geometry of the non-symmetric aneurysm models. L: left, R: right, P: posterior, A: anterior. 23

Table 2.I: Geometric parameters of the different models considered in the study. 24

Figure 2.4: Experimental setup 25

Figure 2.5: Waveform delivered by the pulsatile pump. 26

Figure 3.1: (*a*) Flow waveform input in the pump, (*b*) corresponding velocity profiles across the abdominal aorta at different instants of time in one cardiac cycle. 32

Figure 3.2: Wall shear stresses measured in a model of healthy infrarenal aorta..... 33

Figure 3.3: Comparison of the velocity profiles across the abdominal aorta measured experimentally with the ones calculated with the Womersley solution..... 37

Figure 3.4: Profile of wall shear stresses calculated with the analytical solution in a healthy abdominal aorta over one period. 38

Figure 3.5: Instantaneous velocity field measured in model 4 with the PIV system. 40

Figure 3.6: (*a*) Instantaneous vorticity and (*b*) stress fields measured in model 4 at times B to E, non-dimensionalised by the peak value occurring in the healthy vessel. 41

Figure 3.7: (a) Velocity, (b) vorticity and (c) stress fields, at times B to E, measured in model 4 and phase-averaged over 6 cardiac cycles. 43

Figure 3.8: Zoom measurements of the velocity (*a*), vorticity (*b*) and stress (*c*) fields in the distal area of model 4. 44

Figure 3.9: Instantaneous (*a*) and phase-averaged (*b*) velocity field measured in the transverse cut located at the point of maximum diameter at times C and D. 45

Figure 3.10: Comparison of the phase-averaged velocity field measured with the PIV system in models 1 (*a*), 2 (*b*) and 5 (*c*) at times C and D. 47

Figure 3.11: Comparison of the non-dimensionalized phase-averaged vorticity field measured in models 1 (a), 2 (b) and 5 (c) at times C and D. 48

Figure 3.12: Comparison of the phase-averaged velocity field measured in models 11 (*a*), 6 (*b*) and 1 (*c*) at times C and D. 49

Figure 3.13: Comparison of the non-dimensionalized phase-averaged vorticity field measured in models 11 (*a*), 6 (*b*) and 1 (*c*) at times C and D. 50

Figure 3.14: Maximum position of the core of the vortex ring inside the AAA plotted as a function of the *D/d* and *L/d* ratios. 51

Figure 3.15: Time evolution of the non-dimensionalized, phase-averaged wall shear stresses along the aneurysmal wall in models 1 (*a*), 2 (*b*), 4 (*c*) and 5 (*d*). 53

Figure 3.16: Time evolution of the gradient of the phase-averaged wall shear stresses along the aneurysmal wall in models 1 (*a*), 2 (*b*), 4 (*c*) and 5 (*d*) (in N/m^3). 54

Figure 3.17: Evolution of WSS_{mean} along the aneurysmal wall in models 1 (*a*), 2 (*b*), 4 (*c*) and 5 (*d*). The results are shown only inside the AAA. 55

Figure 3.18: Evolution of WSS_{mag} along the aneurysmal wall in models 1 (*a*), 2 (*b*), 4 (*c*) and 5 (*d*). The results are shown only inside the AAA. 56

Figure 3.19: Evolution of the OSI factor along the aneurysmal wall in models 1 (*a*), 2 (*b*), 4 (*c*) and 5 (*d*). The results are shown only inside the AAA. 57

Figure 3.20: Time evolution of the non-dimensionalized, phase-averaged wall shear stresses along the aneurysmal wall in models 11 (*a*), 6 (*b*) and 1 (*c*). 59

Figure 3.21: Time evolution of the gradient of the phase-averaged wall shear stresses along the aneurysmal wall in models 11 (*a*), 6 (*b*) and 1 (*c*) 60

Figure 3.22: Evolution of WSS_{mean} along the aneurysmal wall in models 11 (*a*), 6 (*b*) and 1 (*c*). The results are shown only inside the AAA. 61

Figure 3.23: Evolution of the *OSI* index along the aneurysmal wall in models 11 (*a*), 6 (*b*) and 1 (*c*). The results are shown only inside the AAA. 62

Figure 3.24: Velocity field calculated with the slowly expanding aneurysm model in an AAA with the same geometry as model 11. 65

Figure 3.25: Wall shear stresses calculated with the slowly expanding aneurysm model in an AAA with the same geometry as model 11. 66

Table 3.I: Comparison of different characteristic quantities, WSS_{max}, WSS_{min}, WSS_{mean}, WSS_{mag} and *OSI*, at 6 positions along the AAA in model 4. 68

Figure 3.26: Time evolution of the wall shear stresses at a few locations inside model 4: y/d = -0.4, 0, 0.75, 1.5, 2.25 and 3. 69

Figure 3.27: Time evolution of the gradients of wall shear stresses at a few locations inside model 4: y/d = -0.4, 0, 0.75, 1.5, 2.25 and 3. 70

Figure 4.1: Instantaneous velocity field measured in model 16 with the PIV system during one cardiac cycle. 78

Figure 4.2: Instantaneous non-dimensionalized vorticity (*a*) and stress (*b*) fields measured in model 16 with the PIV system..... 79

Figure 4.3: Non-dimensionalized phase-averaged velocity (*a*), vorticity (*b*) and stress (*c*) fields measured in model 16 with the PIV system..... 80

Figure 4.4: Non-dimensionalized phase-averaged velocity (*a*), vorticity (*b*) and stress (*c*) fields measured in the symmetric plane in model 17 with the PIV system. 82

Figure 4.5: Non-dimensionalized phase-averaged velocity (*a*), vorticity (*b*) and stress (*c*) fields measured in the symmetric plane in model 18 with the PIV system. 83

Figure 4.6: Non-dimensionalized instantaneous velocity (*a*), vorticity (*b*) and stress (*c*) fields measured in the non-symmetric plane in model 17 with the PIV system..... 85

Figure 4.7: Non-dimensionalized instantaneous velocity (*a*), vorticity (*b*) and stress (*c*) fields measured in the non-symmetric plane in model 18 with the PIV system..... 86

Figure 4.8: (*a*) Instantaneous velocity field in model 18 with $\overline{Re}_m$ = 540, (*b*) non-dimensionalized vorticity field, (*c*) streamlines on velocity magnitude field 87

Figure 4.9: (*a*) Non-dimensionalized phase-averaged WSS in model 16, (*b*) Gradient of the phase-averaged WSS (*c*) Mean WSS, magnitude of the WSS and OSI index. .. 89

Figure 4.10: (*a*) Non-dimensionalized phase-averaged WSS in model 17 (symmetric view), (*b*) GWSS, (*c*) WSS_{mean}, WSS_{mag} and OSI index. 91

Figure 4.11: (*a*) Non-dimensionalized phase-averaged WSS in model 18 (symmetric view), (*b*) GWSS, (*c*) WSS_{mean}, WSS_{mag} and OSI index. 92

Figure 4.12: (*a*) Non-dimensionalized phase-averaged WSS in model 17 (non-symmetric view, posterior wall), (*b*) GWSS, (*c*) WSS_{mean}, WSS_{mag} and OSI index. 93

Figure 4.13: (*a*) Non-dimensionalized phase-averaged WSS in model 18 (non-symmetric view posterior wall), (*b*) GWSS, (*c*) WSS_{mean}, WSS_{mag} and OSI index. 94

Figure 4.14: (*a*) Non-dimensionalized phase-averaged WSS in model 17 (non-symmetric view, anterior wall), (*b*) GWSS, (*c*) WSS_{mean}, WSS_{mag} and OSI index..... 95

Figure 4.15: (*a*) Non-dimensionalized phase-averaged WSS in model 18 (non-symmetric view anterior wall), (*b*) GWSS, (*c*) WSS_{mean}, WSS_{mag} and OSI index..... 95

Figure 4.16: Phase-averaged velocity field measured in the left and posterior planes in the anatomically correct model at time B. 96

Figure 4.17: Phase-averaged velocity field measured in the left view plane in the anatomically correct model at times C and E. 97

Figure 4.18: Instantaneous velocity (*a*) and vorticity fields (*b*) measured at peak systole in model 16 under a sinusoidal flow waveform. 99

Figure 4.19: Phase-averaged profiles of WSS measured in model 18 at *y/d* = 1.7 along the anterior wall (*a*) and at *y/d* = 1.7 and 3 along the posterior wall (*b*). 100

Figure 5.1: Trajectories and stress history for the 10 cells released in model 5 at *y*/d = -0.8 at time C 109

Figure 5.2: (*a*) Velocity and (*b*) and stress profiles across a healthy vessel at the 10 instants of time that compose one cardiac cycle.. 110

Figure 5.3: Trajectories and stress history of cells released in Models 11 (*a*), 6 (*b*) and 1 (*c*) during systole (time C) and *y/d* = -0.8. 111

Figure 5.4: Trajectories of cells released in Models 11 (*a*), 6 (*b*) and 1 (*c*) during diastole (time G) and *y/d* = -0.8. 112

Figure 5.5: Comparison of the residence time, near wall residence time, mean and peak stress and platelet activation factors for models 11, 6 and 1. 113

Figure 5.6: Trajectories and stress history of cells released in Models 2 (*a*) and 4 (*b*) during systole (time C) and *y/d* = -0.8. 115

Figure 5.7: Comparison of the residence time, near wall residence time, mean and peak stress and platelet activation factors for models 1, 2, 4 and 5 116

Figure 5.8: Trajectories and stress history of cells released in Models 17 (*a*) and 18 (*b*) during systole (time C) and *y/d* = -0.8. 118

Figure 5.9: Comparison of the residence time, near wall residence time, mean and peak stress and platelet activation factors for models 5, 17 and 18. 119
Figure 5.10: Comparison of the average values of the residence time, near wall residence time, mean and peak stress and platelet activation factors for all the models. 122
Figure C.1: CT scan images of the abdominal trunk of a patient with an AAA..... 142
Figure C.2: (a) Reconstruction of an AAA from CT scan images, (b) mold generated with a rapid prototyping technique, (c) silicone model built from the mold. 142

ACKNOWLEDGEMENTS

Chapter 3 is, in part, a reprint of the material as it appears in "Evolution of the wall shear stresses during the progressive enlargement of symmetric abdominal aortic aneurysms," Salsac A. V., Sparks S. R., Chomaz J. M. & Lasheras J. C. submitted for publication in Journal of Fluid Mechanics. Chapter 4 contains material of the paper "Effects of the loss of symmetry on the wall shear stresses in abdominal aortic aneurysms," Salsac A. V., Sparks S. R., Chomaz J. M. & Lasheras J. C., submitted for publication in the Journal of Fluid Mechanics. Chapter 5 is, in part, a reprint of the paper "Physiological relevance of the changes in hemodynamics for circulating blood cells in abdominal aortic aneurysms," as it has been submitted for publication in Journal of Biomechanics. The dissertation author was the primary researcher and author in each of these publications and the co-authors listed in these publications directed and supervised the research.

When it comes to acknowledging all the people that counted for me over the years of my Ph.D., so many names come to my mind. I would have loved to leave a personal note to all of you, but I fear it would be too long. So, to keep it short (maybe too short...), I would like to express my gratitude and warmly thank

- Juan, for having given me the opportunity to conduct a Ph.D. and guided me so well along the way, while giving me a lot of autonomy. Thank you for introducing me to the field of Biomechanics and for opening my eyes to all the problems that can still be solved. Thank you also for letting me work in partnership with France.

- Jean-Marc, for having agreed to come onboard of this adventure that has been the joint Ph.D. between UCSD and the Ecole Polytechnique. Thank you for all the discussions we had and for all your help.

- Steve, for explaining me some of the secrets of the human body and for helping me conduct the experiments in joy and good humor.

And to all of you, my dearest friends, thank you for having made my Ph.D the most enriching time of my life.

Finally, I would like to dedicate this dissertation to my parents and to my sister, Marie-Delphine, to whom I owe everything...

VITA

February 19, 1977	Born, Strasbourg, France
2000	Diplôme d'Ingénieurs (Engineering Degree). Ecole Nationale Supérieure d'Hydraulique et de Mécanique de Grenoble (ENSHMG), Institut National Polytechnique de Grenoble (INPG), Grenoble, France
2001–2005	Research and Teaching Assistant. Department of Mechanical and Aerospace Engineering, University of California, San Diego
2001	Master of Science. University of California, San Diego
2002–2005	Joint-Ph.D. with the Laboratory of Hydrodynamics, Ecole Polytechnique, France.
2005	Ph.D. University of California, San Diego
2005	Lecturer, Laboratory class in Materials / Fracture Mechanics, Department of Mechanical and Aerospace Engineering, University of California, San Diego

HONORS AND AWARDS

2000–2001	Irwin and Joan Jacobs Fellowship. Jacobs School of Engineering. University of California, San Diego.
2002	Outstanding Teaching Assistant Award. Department of Mechanical and Aerospace Engineering, University of California, San Diego.
2002–2005	Ph.D. Fellowship. Centre National de la Recherche Scientifique (CNRS), France.
2004	Outstanding Teaching Assistant Award. Department of Mechanical and Aerospace Engineering, University of California, San Diego.
2005	Dissertation Fellowship. Department of Mechanical and Aerospace Engineering, University of California, San Diego.

PUBLICATIONS

Reviewed papers:

Salsac A. V., Sparks S. R. & Lasheras J. C. "Hemodynamic changes occurring during the progressive enlargement of abdominal aortic aneurysms." *Ann. Vasc. Surg.* **18**, 14–21 (2004).

Salsac A. V., Sparks S. R., Chomaz J. M. & Lasheras J. C. "Evolution of the wall shear stresses during the progressive enlargement of symmetric abdominal aortic aneurysms." *J. Fluid Mech.* (submitted) (2004).

Salsac A. V., Sparks S. R., Chomaz J. M. & Lasheras J. C. "Effects of the loss of symmetry on the wall shear stresses in abdominal aortic aneurysms." *J. Fluid Mech.* (submitted) (2005).

Salsac A. V., Sparks S. R., Chomaz J. M. & Lasheras J. C. "Physiological relevance of the changes in hemodynamics for circulating blood cells in abdominal aortic aneurysms." *J. Biomech.* (submitted) (2005).

Book chapter:

Salsac A.-V., Sparks S. R. & Lasheras J. C. "Changes in pressure and wall tension occurring during the enlargement of abdominal aortic aneurysms." *Simplicity, Rigor and Relevance in Fluid Mechanics* (ed. Higuera F. J., Jiménez J. & Vega J. M.). CINME Barcelona (2004).

FIELDS OF STUDY

Major Field: Fluid Mechanics / Engineering

Studies in Fluid Mechanics

Professors Keiko Nomura, Kalyanasundaram Seshadri, Constantine Pozrikidis, Sutanu Sarkar, Larri Armi, Paul Linden, Stefan Llewellyn-Smith and Juan C. Lasheras

Studies in Biomechanics

Professors Andrew McCulloch, Geert W. Schmid-Schoenbein, Paul C. Johnson and Juan C. Lasheras. Doctor Steven R. Sparks

Studies in Environmental Fluid Dynamics

Professors Colm Caulfield and Jim Rottman

Studies in Compressible flows, Physics of Gases and Combustion

Professor Forman Williams

Studies in Numerical Methods

Professors Thomas Bewley and Constantine Pozrikidis

Studies in Methods in Applied Mechanics

Professors Stefan Llewellyn-Smith and Glenn Ierley

ABSTRACT OF THE DISSERTATION

Changes in the Hemodynamic Stresses Occurring During
the Enlargement of Abdominal Aortic Aneurysms

by

Anne-Virginie Salsac
Doctor of Philosophy in Engineering Sciences (Mechanical Engineering)
University of California, San Diego, 2005
Professor Juan C. Lasheras, Chair
Professor Jean-Marc Chomaz, co-Chair

This research seeks to improve the understanding of the mechanisms accounting for the growth of abdominal aortic aneurysms (AAA), by quantifying the role that mechanical stimuli play in the disease processes. In recent years, the development of vascular diseases has been associated with the formation of disturbed patterns of wall shear stresses (WSS) and gradients of wall shear stresses (GWSS). They have been shown to affect the wall structural integrity, primarily via the changes induced on the morphology and functions of the endothelial cells (EC) and circulating blood cells.

Particle Image Velocimetry measurements of the pulsatile blood flow have been performed in aneurysm models, while changing systematically their geometric parameters. The parametric study shows that the flow separates from the wall even at early stages of the disease (dilatation $\leq$ 50%). A large vortex ring forms in symmetric aneurysms, followed by internal shear layers. Two regions with distinct patterns of WSS have been identified: a region of flow detachment, with low oscillatory WSS, and a

downstream region of flow reattachment, where large negative WSS and sustained GWSS are produced as a result of the impact of the vortex ring.

The loss of symmetry in the models engenders a helical flow pattern due to the non-symmetric vortex shedding. The dominant vortex, whose strength increases with the asymmetry parameter, is shed from the most bulged wall (anterior). It results in the formation of a large recirculating region, where ECs are subjected to quasi-steady reversed WSS of low magnitude, while the posterior wall is exposed to quasi-healthy WSS. GWSS are generated at the necks and around the point of impact of the vortex.

Lagrangian tracking of blood cells inside the different models of aneurysms shows a dramatic increase in the cell residence time as the aneurysm grows. While recirculating, cells experience high shear stresses close to the walls and inside the shear layers, which may lead to cell activation. The vortical structure of the flow also convects the cells towards the wall, increasing the probability for cell deposition and ipso facto for the formation of an intraluminal thrombus.

RESUME DE LA THESE

Evolution des Contraintes Hémodynamiques lors de
la Croissance des Anévrismes Aortiques Abdominaux

par

Anne-Virginie Salsac
Doctor of Philosophy in Engineering Sciences (Mechanical Engineering)
University of California, San Diego, 2005
Professeur Juan C. Lasheras, Directeur de thèse
Professeur Jean-Marc Chomaz, co-Directeur de thèse

Cette étude a pour but d'améliorer la compréhension des mécanismes responsables de la croissance des anévrismes aortiques abdominaux (AAA) et plus particulièrement de quantifier les effets des stimuli mécaniques sur la maladie. Des études récentes ont associé la plupart des maladies cardiovasculaires à des changements des contraintes pariétales et de leurs gradients. Toute modification des contraintes hémodynamiques influe l'intégrité structurelle de la paroi, à cause des changements induits sur la morphologie et les fonctions des cellules endothéliales et des cellules sanguines en circulation.

Des mesures PIV (Particle Image Velocimetry) de l'écoulement pulsé ont été réalisées dans des modèles d'anévrismes, dont les paramètres géométriques ont été changés systématiquement. Les résultats de l'étude paramétrique montrent que l'écoulement décolle de la paroi même aux stades très précoces de la maladie (dilatation $\geq$ 30%). Un large anneau de vorticité est formé dans les modèles symétriques

d'anévrismes, suivi de couches de mélange. Deux régions distinctes peuvent être identifiées : une zone de décollement caractérisée par de faibles contraintes oscillantes, et une région distale de réattachement, où de larges contraintes pariétales négatives et des gradients entretenus apparaissent en réponse à l'impact de l'anneau tourbillonnaire sur la paroi.

La perte de symétrie des modèles engendre un écoulement hélicoïdal. Le tourbillon qui domine l'écoulement se détache de la paroi à la courbure maximale (paroi antérieure). Il conduit à la formation d'une zone de recirculation, où les cellules endothéliales sont soumises à des contraintes pariétales négatives et quasi-permanentes avec de très faibles amplitudes, alors que la paroi postérieure est exposée à des contraintes proches de celles d'une aorte saine. Des gradients de contraintes sont générés aux cous de l'anévrisme, ainsi qu'au point d'impact du tourbillon.

Un suivi Lagrangien de cellules sanguines à l'intérieur des différents modèles d'anévrisme montre que l'élargissement de l'anévrisme conduit à une augmentation du temps de résidence des cellules. Lors de leur recirculation, les cellules sont périodiquement soumises à de larges contraintes près de la paroi et dans les couches de mélange, ce qui peut conduire à l'activation des cellules. La structure tourbillonnaire de l'écoulement convecte les cellules vers la paroi, ce qui augmente la probabilité de dépôt des cellules sur la paroi et par conséquent de formation d'un thrombus endoluminal.

Chapter 1

General introduction

An aneurysm is a permanent abnormal bulging of a vessel. Although aneurysms can occur in any type of blood vessels, the great majority of them form in arteries, in only a few restricted localizations. Aneurysms commonly develop along the circle of Willis in the brain and in the abdominal and thoracic portions of the aorta. Intracranial aneurysms tend to be saccular in shape or "berry-like", whereas abdominal (Figure 1.1) and thoracic ones are typically fusiform, many thoracic aneurysms being dissecting[1]. Such a difference in shape indicates that the pathogenesis is likely to be different for each type of aneurysms.

An abdominal aortic aneurysm (AAA) is a spindle-shaped dilatation of the infrarenal abdominal aorta that lies between the renal bifurcation and the iliac branches (Figure 1.2). About one fifth of large abdominal aneurysms are not limited to just the aorta, but have extended to one or both of the common iliac arteries (Armon *et al.* 1998). A localized aortic dilatation is clinically considered an aneurysm, when its maximal diameter is greater than 1.5 times the healthy diameter (Johnston *et al.* 1991).

[1] A dissecting aneurysm occurs when blood gets through a lengthwise tear between layers off the wall of an artery.

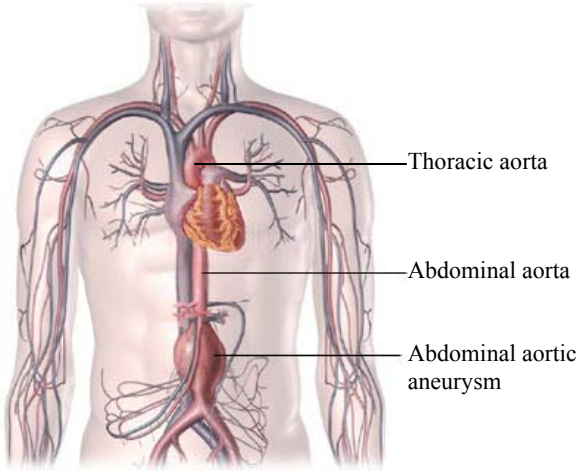

Figure 1.1: Abdominal aortic aneurysm

Aneurysms tend to grow asymptomatically, which explains why AAAs are rarely detected at early stages. Three out of four AAAs show no symptoms at the time they are diagnosed (Szilagyi 1982; Pokrovskii 2003). In some instances, large aneurysms may put pressure on vertebral bodies, causing lumbar pain (Sterpetti *et al.* 1988). The presence of a blood clot inside the AAA, also called endoluminal thrombus, may lead to emboli, when fractions of it break off and become lodged downstream in a smaller vessel. Otherwise, physicians must rely on non-invasive imaging techniques such as ultrasound, computed tomography (CT), or magnetic resonance imaging (MRI) to accurately determine the presence and extent of the aneurysmal disease (Figure 1.3).

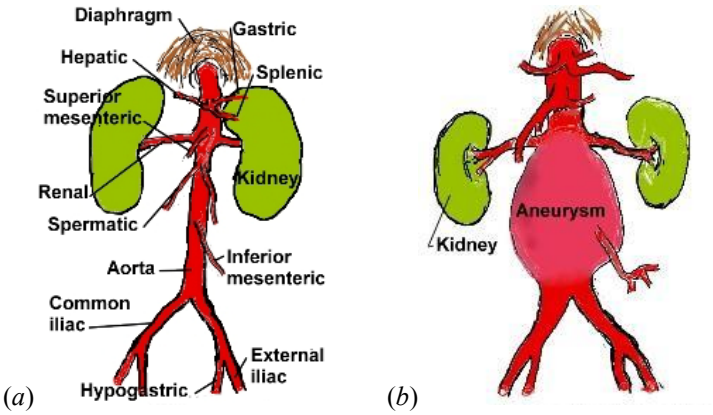

Figure 1.2: (*a*) Anatomy of the abdominal trunk, (*b*) Abdominal aortic aneurysm

Similarly to other vascular diseases, the rate of incidence of AAAs has increased over the last decades, which partly reflects the rise in the population life expectancy, but probably also the improvements made in diagnostic tools (Reilly & Tilson 1989; Best, Price & Fowkes 2003). It is estimated that 2-3% of the population over age 50 have an occult abdominal aortic aneurysm (Collin & Radcliffe 1988; Bonamigo & Siqueira 2003) and 200,000 new aneurysms are diagnosed each year in the United States. The incidence in males increases after age 55 with a peak in the seventh decade. In females, the incidence begins to rise at a later age (greater than age 70) with a continuous increase until the time of death (Bengtsson *et al.* 1996). The current male to female ratio for death from AAA has been reported to be as high as 11:1 between ages 60 an 64, and narrows to 3:1 between ages 85 and 90 (Collin & Radcliffe 1988).

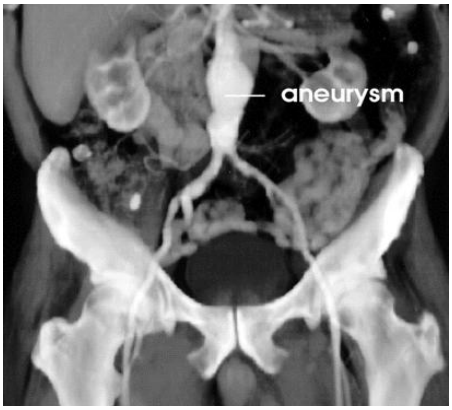

Figure 1.3: Spiral computed tomography (CT) with 3-D reconstruction showing an abdominal aneurysm originating below the renal arteries

Once formed, an aneurysm typically continues to enlarge progressively and at some point may rupture causing life-threatening bleeding. The overall mortality rate for ruptured AAA is 60-80%, which drops to 30-65% if the patient reaches a hospital alive (Ingoldby *et al.* 1986; Samy, Whyte & MacBain 1994; Basnyat *et al.* 1999; Singh *et al.* 2001). AAAs are responsible for 15,000 deaths annually in the United States, representing the 13th leading cause of death in the country (Reilly & Tilson 1989). But

misdiagnosed ruptured aneurysms are probably responsible for many additional cases of sudden death in older persons.

No accurate technique exists to date to either predict the aneurysmal expansion rate or its critical size or shape at the point of rupture. Treatment of AAA is decided on the basis of several factors, including size, expansion rates, natural history data and operative morbidity and mortality rates (Stringfellow, Lawrence & Stringfellow 1987; Hughes & Fontenelle 2000). It is widely recognized that increase in size leads to a higher risk of rupture (Law, Morris & Wald 1994; Englund *et al.* 1998). The average annual rupture rate of an aneurysm measuring < 4 cm is 0%, 1% when 4.5 cm, 11% when 5.5 cm and 26% when 6.5 cm (Green 2002). Although the likelihood for a small size aneurysm to rupture is very small, Darling (1970) proved that it can happen. Treatment is currently recommended for AAAs exceeding 5 cm in maximal diameter (Taylor & Porter 1985; Prisant & Mondy 2004) or having an enlargement rate greater than 0.5 cm in six months (Treska & Certik 1999), leaving the management of small AAAs (< 5 cm diameter) in an area of continuing controversy.

A. Changes in the wall composition involved in the formation, enlargement and rupture of AAAs

Except the capillaries, which are only one cell thick, all the vessel walls are composed of 3 layers (or "tunica"), the adventitia, the media and the intima (Figure 1.4). The thickness and proportion of components of each layer vary depending on the function of the vessel, arteries having thicker, more muscular and elastic walls than veins. In the case of arteries, (*i*) the adventitia, the outermost layer, is largely composed of ground matter, collagen bundles, some elastin fibers, autonomic nerves and small blood vessels (or "vasa vasorum") that irrigate the adventitia. In the thoracic aorta, small branches of the vasa vasorum extend into the tunica media, but in the abdominal aorta,

the media only relies on diffusion processes to receive oxygen and nutrients from the lumen. (*ii*) The media is composed primarily of waves of smooth muscle cells (SMC) intermixed with elastin sheets, embedded in an extra-cellular matrix. It accounts for most of the strength and elasticity of the arterial wall and for the dynamic-recoil property of the wall. During systole, the elastic walls stretch to accommodate the volume of blood ejected from the heart, then recoil acting as a second subsidiary pump. (*iii*) The intima is composed of a lining mono-cell layer of multifunctional vascular endothelial cells (EC) that sits on a basal lamina and a very thin layer of connective tissue.

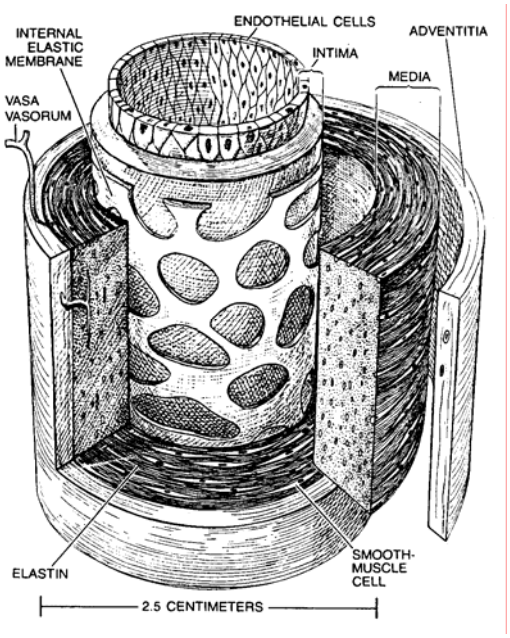

Figure 1.4: Wall composition of an arterial wall (Johansen 1982)

Smooth muscle cells and endothelial cells are the main cellular components of the arterial wall. The SMC play an important role in the development and maintenance of the arterial wall structure. They are the main source of collagen, elastin and other extra-cellular matrix components, such as proteoglycans, whose function includes regulation of cell adhesion, migration and proliferation. Endothelial cells at the interface between the blood flow and the wall act as a permeable barrier blocking the passage to large

molecules. They also detect and signal vascular injury and regulate the structure and function of the smooth muscle cells by producing vasoactive substances (NO, prostacyclin, etc.). The actuation of the contractile tone of the muscle cells is achieved by EC sensing the mechanical forces (pressure and shear stresses) acting on them, a process known as "mechanotransduction".

Several factors may account for the much higher incidence of aneurysms in the abdominal aorta than in the thoracic segment (Best, Price & Fowkes 2003). The abdominal aorta is characterized by a smaller number of elastic lamellae in the medial layer than the thoracic aorta and therefore has a higher elastic modulus (Dobrin 1989; Nichols 1998 pp. 91-92). The pressure pulse is modified as it progresses along the aorta, as a result of the tapering of the aorta, stiffening of the aortic wall and presence of bifurcating branches, which leads to reflections of the pressure wave. Although the mean pressure decreases gradually, the pressure at peak systole largely increases as well as the temporal pressure gradient (McDonald 1974; Pedley 1979; MacSweeney 1993). The typically stiffer walls and higher systolic pressure of the infrarenal aorta may play a role in the pathogenesis of AAAs. Disruption of the elastin sheets has been thought to be the first step in the aneurysm formation. Aneurysm formation has been shown to occur after the sole induction of elastin failure in the tunicae media and adventitia (White & Mazzacco 1996).

AAAs develop primarily in older people and in an elastic artery that has undergone structural changes. With aging, a generalized process of increasing arterial stiffness results from the progressive replacement of elastin by collagen in the walls of large arteries (O'Rourke 1990). Arterial-related stiffening further leads to an increase in arterial pressure (Izzo & Shykoff 2001). Over time, the iliac bifurcation evolves in shape (Sun *et al.* 1994) and the lumen cross-section area of the common iliac arteries tends to decrease substantially (Hardy-Stashin, Meyer & Kauffman 1980; Greenwald, Carter &

Berry 1990). Besides, the iliac arteries are prone to atherosclerosis (Shah, Scarton & Tsapogas 1978; Pedersen, Yoganathan & Lefebvre 1992), which further decreases the size of the iliac lumen. This results in a higher systolic pressure in the infrarenal aorta, increasing the potential for AAA formation. These mechanisms could explain the relationship found by Matsushita *et al.* (2000) between aortic calcification and atherosclerotic disease in patients with AAAs.

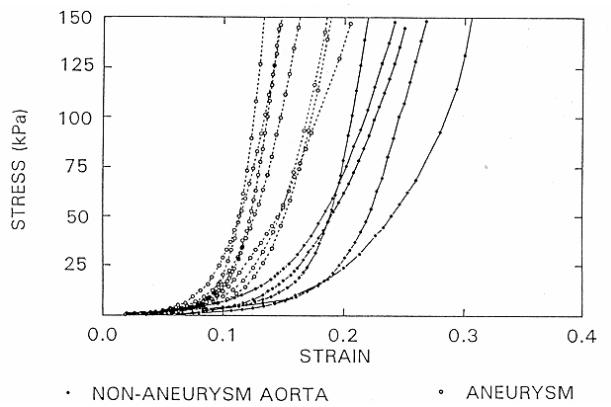

Figure 1.5: Elastic diagram of normal (dark circle) and aneurysmal (open circle) aortic walls. Shift of the curves corresponding to aneurysmal walls (He & Roach 1994).

Once the AAA is formed, it is characterized by profound changes in the aortic wall composition. Elastase activity and also collegenase later on in the disease process are increased within the aneurysm wall (Busuttil, Abou-Zamzam & Machkeder 1980; Busuttil *et al.* 1982; Carmo *et al.* 2002). The elastin-collagen ratio increases, further increasing the wall stiffness (Sumner, Hokanson & Strandness 1970; MacSweeney *et al.* 1992; He & Roach 1994; Thubrikar *et al.* 2001) – see Figure 1.5. The marked stiffness leads to little oscillatory deformations of the walls. The lack of stimulation on the smooth muscle cells results in a reduction in the synthesis of connective tissues in the media or even in the possible apoptosis of the cells (López-Candales *et al.* 1997; Thompson, Lias & Curci 1997; Liao *et al.* 2000). The depletion in matrix proteins is partially compensated by synthesis mechanisms that take place in the adventitia (Ghorpade &

Baxter 1996). The inflammatory response, indissociable of AAAs, is believed to play a key role in the structural degeneration of the elastic media. Inflammatory leukocytes infiltration into the wall and secrete proteolytic enzymes and effector molecules that destroy the matrix and affect its synthesis (Ghorpade & Baxter 1996).

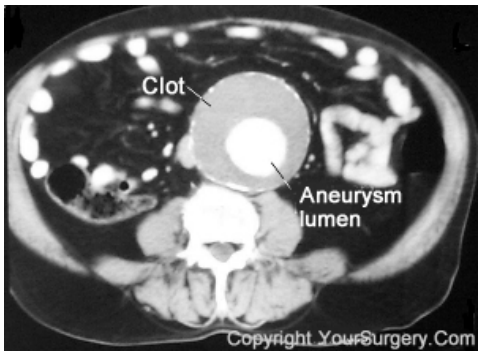

Figure 1.6: CT scan through an 8.5-cm AAA. The thrombus has filled most of the cavity, leaving a lumen with a diameter close to the size in a healthy vessel. (YourSurgery.com)

The endoluminal thrombus that lines the lumen of later-stage aneurysms may also play an important role in the enlargement of AAAs, although it is still undetermined (Figure 1.6). A mural thrombus develops in 75% of the aneurysms with a maximum diameter greater than 4.5 cm (Harter *et al.* 1982). The solid fibrin structure, in which platelets, blood cells, proteins and debris are imbedded, obstructs part of the lumen, restoring in most cases the original lumen diameter. Although no consensus has been reached on the ability of the thrombus to transmit pressure to the wall, all the studies agree that the thrombus reduces the wall stress by its ability to sustain tensile loads, adding structural support to the wall (Mower, Quinones & Gambhir 1997; Inzoli *et al.* 1993; Di Martino *et al.* 1998; Schurink *et al.* 2000; Mower & Quinones 2001; Thubrikar *et al.* 2003; Chaudhuri *et al.* 2004). Wang *et al.* (2001) have derived a two-parameter, large-strain, hyperelastic constitutive model, based on their uniaxial tensile testings. They have shown that the thrombus is made of three layers: the luminal layer, arranged in thick fibrin bundles, has the highest stiffness and strength. These fibers are respectively

partially and completely degenerated in the medial and abluminal layers. The thrombus is likely to act as a barrier to oxygen and nutrient diffusion to the intima and media layers (Vorp *et al.* 1998; Vorp *et al.* 2001), making the aneurysm wall prone to ischemia. Kazi *et al.* (2003) showed that the thrombus causes a marked reduction in wall thickness and more frequent signs of inflammation in the wall. Leukocytes that accumulate in the thrombus generate inflammatory enzymes (proteases) that further affect the wall structural integrity (Satta, Laara & Juvonen 1996; Adolf *et al.* 1997; Gacko & Głowiński 1998; Fontaine *et al.* 2002; Wang *et al.* 2002).

B. Pathogenesis of the abdominal aortic aneurysms

Although the pathogenesis of AAAs is thought to be multi-factorial and predominantly degenerative, the exact mechanisms responsible for the etiology of AAAs are not established. Several risk factors have, however, been shown to play a role in the formation of the disease. Some of the risk factors, such as age and gender (Singh *et al.* 2001; Bengtsson, Sonesson & Bergqvist 1996) or family history (Noorgard, Rais & Angquist 1984; Reilly & Tilson 1989; Salo *et al.* 1999) can be considered inevitable. We already discussed that AAAs are associated with aging processes and specificities to the male gender. The observed family occurrence of AAAs makes plausible the existence of a genetic link involved with the degeneration of the aortic wall and the development of AAAs, but no genetic factor has yet been discovered. Two rare hereditary disorders are known to promote the formation of aneurysms: Marfan's and Ehlers-Danlos' Syndromes (Wilmink *et al.* 2000). Marfan's Syndrome causes an abnormal breakdown of the elastic fibers in the aortic wall. Ehlers-Danlos syndrome is the name given to a group of inherited disorders that involve a genetic defect in collagen and connective tissue structure and synthesis. But these diseases tend to be rather associated with thoracic aneurysms than with AAAs.

Similarly to other cardiovascular diseases such as atherosclerosis, other predisposing risk factors are high blood pressure (Treska & Certik 1999; Pokrovskii *et al.* 2003), smoking (UK trial 2000) and high cholesterol (Singh *et al.* 2001). Hypertension affects all parts of the cardiovascular system. Local cells, such as endothelial cells and smooth muscle cells that sense the level of the hemodynamic forces (pressure and shear stresses) and transduce the signals into vasomotor responses are directly affected by the increase in blood pressure. Hypertension has been shown to distend the aorta (Paivansalo *et al.* 2000) and thicken the tunica media (Limas, Westrum & Limas 1980). As discussed in the previous section, the infrarenal aorta may be even more sensitive to hypertension than other vessels due to its higher inherent stiffness and the presence of the aortic bifurcation downstream of it. Cigarette smoking has been found to be the most important risk factor for the development (Reilly & Tilson 1986), expansion (MacSweeney *et al.* 1994) and rupture (UK trial 2000) of AAAs, aneurysms being 8 times more frequent in smokers than nonsmokers (Auerbach & Garfinkel 1980). Stefanadis *et al.* (1997 & 1998) showed that tobacco smoke leads to an active stiffening of the vessel due to its effect on the endothelial cells and sympathetic nerves resulting in an elevated muscular tone.

AAAs have long been thought to be secondary to atherosclerotic degeneration of the abdominal aorta. However, this view has been challenged over the past 2 decades (Johansen 1982). Atherosclerosis neither explains the high levels of elastase, collagenase and antiproteases nor the extent of the inflammatory processes, hallmarks of AAAs. It is now believed that atherosclerosis may promote aneurysm formation but does not have a causal effect (Lee *et al.* 1997), since only 25% of AAA patients present atherosclerosis (Zarins & Glagov 1982). Among other effects, atherosclerosis may weaken the infrarenal wall itself by reducing the medial thickness and the number of elastin sheets (Zarins, Xu & Glagov *et al.* 2001) and change the pressure waveform when affecting the iliac arteries (see previous section).

C. Influence of the hemodynamic forces on the pathology of AAAs

In recent years, understanding the etiology and progression of AAAs has become a multidisciplinary effort. The research on atherosclerosis has shown that the formation of regions of the vasculature presenting a complex morphology (such as bends, bifurcation, branches as well as sudden expansions and partial occlusions) and complex flow are the most important factors in the pathogenesis of the disease (Fox & Hugh 1966; Ku *et al.* 1985; Yoshida *et al.* 1987; Glagov *et al.* 1988; Lei, Kleinsteuer & Truskey 1995; Pedersen *et al.* 1997; Malek, Alper & Izumo 1999). Numerous investigations have reported the atherogenic effects of altered shear stresses on the vessel walls. This study is therefore based upon the postulate that changes in the hemodynamic forces play a crucial role in the formation and enlargement of AAAs, initiating biochemical events in the arterial wall that may account for the development of the vascular disease. Endothelial cells, smooth muscle cells and circulating cells (*e.g.* platelets) have all been proven to react to hemodynamic forces. Changes in the mechanical forces acting on the cells have the potential to modify their metabolism and function, which can in turn induce profound modifications of the wall composition and integrity.

1. Endothelial cells

ECs have been found to be highly responsive to wall shear stresses (WSS) (Davies *et al.* 1984). Shear stress, rather than pressure or wall tension is the mechanical stimulus that plays the major role (Traub & Berk 1998)[2]. Perturbations from the baseline stress conditions alter the mechanisms of mechanotransduction, changing the cell shape (Helmlinger *et al.* 1991), regulatory functions (Dewey *et al.* 1981; Noris *et al.* 1995) and

[2] It is essential to know that ECs primarily react to shear stresses rather than pressure variations, since the order of magnitude of the pressure variations ($\Delta p \sim 1/2\rho U^2 \sim 10^2$ N/m^2) is much greater than that of the shear stresses (WSS ~ 1 N/m^2).

gene expression of the ECs (Topper *et al.* 1996; Fisher *et al.* 2001; García-Cardeña[1] *et al.* 2001; Blackman, García-Cardeña & Gimbrone 2002; Tzima *et al.* 2002; Warabi *et al.* 2004). It has been shown that ECs not only sense WSS but can also differentiate among different types of stimuli (Helmlinger, Berk & Nerem 1995, García-Cardeña[2] *et al.* 2001). Almost all the studies, mentioned in this paragraph, have been conducted in vitro on endothelial cells cultured alone on a substrate. Therefore, these studies did not take into account the interaction with other types of cells.

In regions of low and oscillating stresses, loss and desquamation of endothelial cells have been observed (Walpola, Gotlieb & Langille 1993). The cells become randomly oriented in all directions, when they align parallel to the main flow direction in a healthy vessel (Levesque & Nerem 1985) (Figure 1.7). Their more rounded shape increases the inter-cellular space and ipso facto, the permeability of the membrane (Helmlinger *et al.* 1991). The absence or drastic reduction in WSS upregulate all the pathophysiologically relevant gene expressions of the endothelial cells. Low and oscillating shear stresses and static flow conditions have been shown to induce the endothelial gene expression of adhesion molecules (Chappell *et al.* 1998; Chiu *et al.* 2003), which, in turn, increases the leukocyte extravasation into the inflamed tissues. They increase the gene expression for platelet-derived growth factor (PDGF) (Kraiss *et al.* 1996), which acts as an important mitogen (*i.e.* induces mitosis) for smooth muscle cells leading to their proliferation and migration (Heldin & Westermark 1999). They also attenuate the EC gene expression of endothelial nitric oxide synthase (eNOS) (Chiu *et al.* 2003). One of the culprits in the pathogenesis of endothelial dysfunctions is the imbalance generated by low shear stress conditions between nitric oxide, a vasodilator, and angiotensin II, a vasoconstrictor. Indeed, nitric oxide is a growth inhibitor and is anti-inflammatory and anti-thrombotic, while angiotensin II is a growth promoter and is pro-inflammatory (Emerson *et al.* 1999).

High shear stresses, on the contrary, increase the nitric oxide release, which tends to lead to a structural expansion of the vessel (Ben Driss *et al.* 1997). This phenomenon may be viewed as an attempt to restore the WSS back to their healthy level (Kamiya & Togawa 1980; Zarins *et al.* 1987). In the regions of transition to turbulence, the turnover of the endothelial cells increases drastically (Davies *et al.* 1986), which does not occur in regions of laminar oscillating flow, although they are both characterized by multi-directional fluctuating patterns of shear stresses. The mechanisms initiating endothelial turnover in turbulent flow conditions remain therefore unexplained.

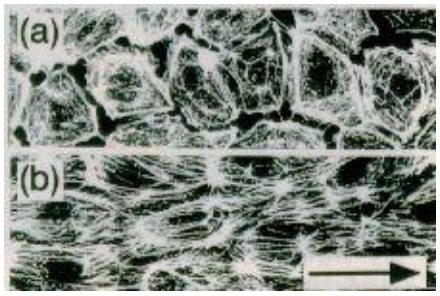

Figure 1.7: Morphology of endothelial cells (*a*) before and (*b*) after applying shear stress (M. Sato)

ECs are also sensitive to the spatial (Davies, Mundel & Barbee 1995) and temporal (Blackman, Thibault & Barbee 2000) gradients of wall shear stresses. High spatial gradient regions increase the division rate of the cells, which tend to migrate away from these regions by predominantly moving further downstream (DePaola *et al.* 1992). Cell loss is increased around the zone of high WSS gradients, which suggests that a cell proliferation-migration-loss cycle takes place in the vicinity of high gradient regions (Tardy *et al.* 1996). The endothelial cells expression has been shown to be modulated both by the magnitude of the spatial (Nagel *et al.* 1999) and temporal (Bao, Lu & Frangos 1999; Zhao *et al.* 2002) gradients of WSS. The latter also accelerate the remodeling (elongation/alignment) of the endothelial cells (Hsiai *et al.* 2002).

2. Smooth muscle cells

Mechanical stimuli, such as strain and fluid shear stress, influence the function of the smooth muscle cells. Mechanical strain influences the SMC functions, regulating the synthesis of extra-cellular matrix components (Lee *et al.* 2001). WSS modify the cell morphology and organization of the cytoskeleton (Sterpetti[1] *et al.* 1992; Cucina *et al.* 1996). Contrary to the endothelial cells that align with the applied WSS, vascular smooth muscle cells arrange in the direction perpendicular to them (Lee *et al.* 2002; Chiu *et al.* 2004). The existence of a physical link between ECs and SMCs has been demonstrated by Spagnoli *et al.* (1982), so it is plausible that the ECs and SMCs react symbiotically to shear stresses.

In the case of endothelial injury and denudation, SMCs are directly exposed to blood flow. Wang & Tarbell (1995) showed that, in a healthy patient, SMCs may also experience some level of WSS as a result of the transmural flow. Although the interstitial flow is very small, the WSS induced can be of the order of 0.1 to 0.3 N/m^2, which is still lower than the WSS experienced by the ECs. WSS modify the gene expression of the SMC (Papadaki[1] *et al.* 1998) and stimulate the release of platelet-derived growth factor (Sterpetti[2] *et al.* 1992), basic fibroblast growth factor (Rhoads, Eskin & McIntire 2000) and nitric oxide (Papadaki[2] *et al.* 1998; Gosgnach *et al.* 2000).

3. Circulating cells

Hemodynamic forces also have an important effect on the functions of platelets and leukocytes (neutrophils, monocytes and lymphocytes), which are the primary cells involved in the mechanism of thrombosis. Thrombosis is mainly triggered in the case of vascular injury, when the subendothelial or medial layers of blood vessels are in direct contact with the blood, exposing collagen (extrinsic pathway of blood coagulation). But it has long been known that the process of thrombosis depends on blood flow conditions

and convective mass transfer. High shear stresses, very low shear stresses (such as in areas of flow recirculation or stagnation) and large gradients of shear stresses affect the rate and localization of platelet activation/accumulation (Dintenfass 1964; Grabowski 1995). Activation refers to changes in the platelet functions triggered by chemical (thrombin, collagen, etc.) or mechanical stimuli (shear stresses). Upon activation, blood platelets undergo dramatic morphological and biochemical changes, resulting in shape change (extrusion of pseudopods), aggregation and granule secretion.

Most of the investigations on thrombus formation have concentrated on the effects of the lumen obstruction (stenosis) by an atherosclerotic plaque on platelet adhesion and aggregation (Mailhac *et al.* 1994; Tsao *et al.* 1995; Wootton *et al.* 2001; Einav & Bluestein 2004; Bluestein *et al.* 2004, etc). Hence, the vast majority of flow studies on endothelial cells comprise (very) high shear stress conditions. High shear alone has been shown to directly induce platelet activation and aggregation in the case of vessels with intact endothelial cells (Moake *et al.* 1986; O'Brien 1990; Kroll *et al.* 1996; Andrews *et al.* 2001; Shankaran, Alexandridis & Neelamegham 2003). These shear-induced platelet activation and aggregation involve plasma von Willebrand factor (vWF) as the ligand binding platelets to platelets (intrinsic pathway of blood clotting). Chemical stimuli, such as adenosine diphosphate (ADP) (Ikeda *et al.* 1991) and Ca^{2+} (Chow *et al.* 1992) are necessary for shear-activation to occur and they can modulate the effects of the mechanical forces. Shear stress-activation and aggregation are a function of both the shear stress magnitude and the duration that platelets are subjected to the shear stresses (Hellums & Hardwick 1981; Kunov, Steinman & Ethier 1996; Jesty *et al.* 2003). Zhang *et al.* (2003) have shown that platelets are aggregated in response to a 10 N/m^2 stress applied for periods about 10-20 s but minimally activated and rapid disaggregation follows the pulse of high shear (see also Wurzinger *et al.* 1985). Pulses longer than 20 s are required for irreversible aggregation. This suggests that, in vivo, high shear alone

may not be sufficient to induce platelet activation (Goldsmith 1974) or aggregation, even though shear-induced platelet aggregation has been found to be greater in response to pulsatile than steady stimulation (Sutera *et al.* 1988).

Platelets aggregate, however, after a high stress pulse (2.5 s), when exposed to low shear stresses immediately after (Zhang *et al.* 2002). In vivo, aggregation is therefore possible when platelets are entrained into recirculation regions with low secondary flows after high shear stress stimulation (Purvis & Giorgio 1991). Stagnation point flows are, for example, ideal candidates to promote platelet adhesion and subsequent aggregation even upon intact endothelial monolayers (Reininger, Korndorfer & Wurzinger 1998; Lee, Chiu & Jen 1999; David, Thomas & Walker 2001). The convection patterns promote aggregation by bringing platelets in contact with the endothelial surface (Karino & Goldsmith 1984). In the low shear regions, platelet aggregation is mediated by fibrinogen (Ikeda *et al.* 1993). Slow recirculation or stagnation regions induce long residence times and promote cell-cell collisions (Huang & Hellum 1993; Stroud, Berger & Saloner 2000). Platelet may recirculate in the separated region long enough to become activated and form small aggregates. Recirculating regions may also contain higher platelet-activating substances, promoting thrombus formation (Folie & McIntire 1989).

Platelet activation in regions of acute vascular injury is also regulated by the hemodynamic flow rate. The range of shear stress over which platelet adhesion and subsequent aggregation are observed is approximately 0.1 to 20 N/m^2 (Kroll *et al.* 1996). In low flow conditions, upregulated platelet activity results from increased exposure time to subendothelium collagen (Bassiouny *et al.* 1998). At high shear stresses (> 3 N/m^2), vWF acts as the ligand in the platelet thrombus production (Baumgartner, Turitto & Weiss 1980; Baumgartner, Tschopp & Meyer 1980).

Furthermore, recent evidence shows that circulating leukocytes respond not only to humoral inflammatory mediators but also to fluid shear stress (Rosenson-Schloss, Vitolo

& Moghe 1999; Eriksson *et al.* 2000; Marschel & Schmid-Schoenbein 2002). Shear stresses may activate leukocytes by increasing the actin polymerization and aggregation rate (Okuyama *et al.* 1996; Hernandez *et al.* 2001). Circulating leukocytes activate in regions of quasi flow stasis, projecting pseudopodia and increasing the probability of adherence to the vessel wall (Lawrence *et al.* 1997; Moazzam *et al.* 1997). But Moazzam *et al.* (1997) proved that, upon restoration of flow, the shear stresses induce the retraction of the pseudopodia. In response to inflammatory stimuli (e.g. activated endothelial cells (EC)), leukocytes roll along the endothelium and firmly attach before migrating into the vessel wall. The activation of platelets has been shown to greatly affect the interaction between leukocytes and EC. Platelet activation enhances the expression of some adhesion molecules and the gene expression in leukocytes and endothelial cells (Forlow, McEver & Nollert 2000; Fukuda *et al.* 2000; Nomura *et al.* 2001).

D. Hemodynamics in abdominal aortic aneurysms

Owing to their effect on the endothelial cells, smooth muscle cells and circulating cells, the patterns of shear stresses in AAAs appear to be one of the most physiologically relevant parameters to characterize in order to improve the current understanding of the pathogenesis of the disease.

Due to the complexity of measuring the flow inside an aneurysm, there has been no successful attempt at measuring the internal or wall shear stresses *in vivo* inside an abdominal aortic aneurysm. None of the current radiological imaging techniques (MRI, ultrasound, etc.) has a high enough spatial resolution to provide a reliable measurement of the velocity field, let alone of the shear stresses.

Consequently, over the last decade, a fairly large number of studies have been conducted using *in vitro* models to investigate the hemodynamics in AAAs. These studies have been performed in both symmetric and non-symmetric idealized-shape models of

AAA. Many of the studies involve steady flows (Schrader *et al.* 1992; Budwig *et al.* 1993; Peattie *et al.* 1994; Asbury *et al.* 1995; Bluestein *et al.* 1996; Peattie *et al.* 1996; etc.), which is not relevant to the problem at hand, since the flow is highly pulsatile in the aorta. Others (Yu 1999; Yu 2000; Yu & Zhao 2000) measured the velocity field in AAAs for unsteady flows, but used a sinusoidal waveform instead of a physiologically correct waveform, which strongly affects the characteristics of the flow. Finally, Taylor & Yamaguchi (1994) reproduced the flow waveform measured in the ascending aorta of the dog, which differs from the human aortic waveform.

Fukushima, Matsuzawa & Homma (1989) were the first to investigate the pulsatile nature of the flow, reproducing the physiologically correct velocity waveform. They studied experimentally the influence of the geometry of the bulge in three axisymmetric models of AAA, in the range of mean Reynolds numbers $289 \leq \langle \overline{Re} \rangle \leq 748$ and Womersley numbers $4.07 \leq \alpha \leq 10.6$. They showed that the flow remained attached to the walls during the acceleration (systole), but detached at the onset of the deceleration (beginning of diastole), generating a large primary vortex, followed by a weaker secondary vortex, and a recirculation zone dominated by very low velocities. Although this study showed qualitatively the most significant hemodynamic changes occurring as a result of the bulging, it did not provide any measurement of the most physiologically relevant parameters, i.e. the internal and wall shear stresses. As far as the WSS are concerned, a numerical simulation of the idealized laminar flow inside the AAA was realized and showed that, with the exception of the distal area, where the WSS peaked to a value of 1.5 Pa, the aneurysm wall was characterized by low WSS.

A similar qualitative study was conducted by Egelhoff *et al.* (1999) in four symmetric and one non-symmetric models of AAAs, but they did not perform measurements of the WSS either. Measuring the WSS experimentally is challenging, since it requires a precise measurement of the velocity at points very close to the wall, in order to assess the

velocity gradient at the wall. Yip & Yu (2001, 2002) published one set of Laser Doppler Anemometry measurements of WSS. However, they could not measure the spatial distribution of WSS, which is believed to be one of the most important factors leading to physiological changes.

A few groups performed numerical studies of the velocity field and WSS in AAAs. However, most numerical studies have concentrated on the calculation of the wall stresses and have not modeled the flow inside the aneurysm (Raghavan & Vorp 2000; Raghavan *et al.* 2001; Stringfellow, Lawrence & Stringfellow 1987; Thubrikar, al-Soudi & Robicsek 2001, etc.). Di Martino *et al.* (2001) have been the first one to conduct a fluid-structure interaction study. Numerical calculations have difficulty in predicting correctly the flow separation as well as the transition to turbulence, which are the two important characteristics of the aneurysmal flow. Some studies studied non-realistic flow waveform (reproduced non-realistic geometries, such as Viswanath, Rodkiewicz & Zajac (1997) who modeled extremely large AAAs (6 cm $\leq D \leq$ 14 cm) or Finol & Amon (2001), Finol & Amon[1] (2002) and Finol & Amon[2] (2002) who modeled a double aneurysm, made out of two consecutive expansions. Finol et al. (2003), however, completed a three-dimensional numerical simulation of the flow in a few AAA models increasing the asymmetry parameter. Although they showed the formation of detached regions and vortices in one of the non-symmetric models, they did not show their effect on the patterns of WSS, limiting their discussion to the peak systole, when the flow is still fully attached to the walls.

E. Objectives of the study

The above studies, both experimental and numerical, provide a good qualitative description of the flow in an AAA. However, no comprehensive quantitative study of the

evolution of the flow field as the AAA enlarges has been reported and, more importantly, there has been no accurate measurement of the changes in the mechanical stimuli on the endothelial cells and circulating blood cells during the growth of the aneurysm. The aim of this study is therefore to conduct precise measurements of the spatial and temporal changes in the wall shear stresses and internal shear stresses, which are respectively acting on the endothelial and circulating cells. The objective is to quantify their evolution during the progressive enlargement of AAAs.

In the following, we will discuss the results of a parametric study, in which the flow characteristics were studied inside the aneurysm, while varying systematically the geometric parameters of the models. Quantitative measurements of the velocity field inside the AAA models are obtained using Particle Image Velocimetry (PIV), while reproducing a physiologically correct pulsatile flow waveform. The hemodynamic stresses are calculated both internally and at the walls from the measured velocity field.

F. Structure of the dissertation

Chapter 2 presents the experimental setup and method for the in-vitro hemodynamic study. Measurements of the spatial and temporal changes of the wall shear stresses resulting from the aneurysm growth are discussed in Chapters 3 and 4. The measurements have been conducted respectively in symmetric and non-symmetric models of abdominal aortic aneurysms. In order to validate the experimental measurements of the WSS, an analytical model of the flow inside a vessel (healthy aorta or AAA), based on the well-known Womersley solution, is also presented in Chapter 3. Chapter 5 describes the changes in shear stresses acting on circulating blood cells, and Lagrangian changes in the shear stresses acting on them are analyzed as a function of the AAA geometry.

Chapter 2

Methods

A. Experimental apparatus

1. Aneurysm models

The hemodynamics inside an aneurysm depends on the flow characteristics (cardiac output, blood pressure, cardiac rate) and on the geometry of the bulge. In order to characterize the changes in the hemodynamic forces as the aneurysm enlarges, we have conducted a parametric study, in which we have varied the size and symmetry parameters of the aneurysmal dilatation. The experimental study is based on the use of *in vitro* aneurysm models, all fusiform in shape. The models consist of an expansion blown in a straight tube. The effect of the lumbar curvature has been not considered in the present study (Ku & Zhu 1997). This limitation will be further discussed at the end of Chapter 3.

Both symmetric and non-symmetric models have been considered. Incipient aneurysms tend to be symmetric in shape. But aneurysms with a maximum diameter greater than 4 cm typically expand non-symmetrically, because of the presence of the spinal column (Figure 2.1).

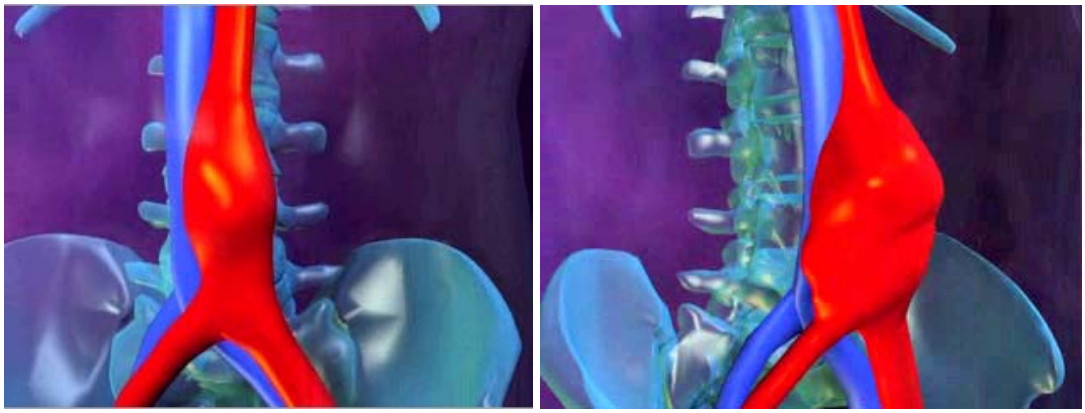

Figure 2.1: Sketches of a small ($D < 4.5$ cm) and later stage aneurysm

The geometry of the models can be characterized by three parameters: the dilatation ratio (D/d), the aspect ratio (L/d) and the asymmetry parameter $\beta = 2e/d$, where D and L are respectively the maximum internal diameter and the length of the aneurysm, d the internal diameter of the parent vessel and e the eccentricity (see Figure 2.2 for the symmetric models and Figure 2.3 for the non-symmetric ones). The eccentricity is defined as the distance between the axis of symmetry of the parent vessel and the centerline at the maximum bulge diameter. The asymmetry parameter β ranges from zero for a symmetric aneurysm to one for a non-symmetric model with a flat posterior wall.

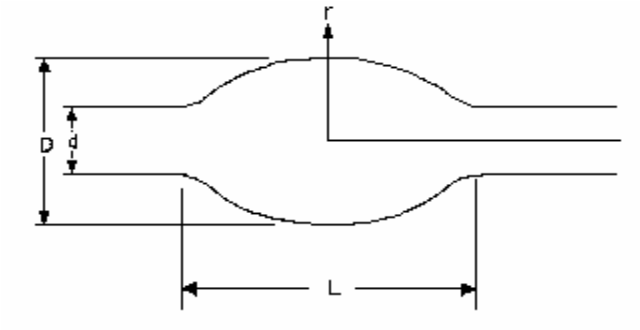

Figure 2.2: Geometry of a symmetric aneurysm model.

In the experiment, these three parameters have been systematically varied in order to study the effects of the aneurysm growth on the hemodynamic forces. Table 2.I summarizes the characteristics of the models considered in the study. The choice of an

idealized geometry for the models was made in order to control their shape with only three parameters. Although the models are not physiologically correct in shape, we hope that all the important physical processes can be observed and measured accurately. The models are supposed to be devoid of an endoluminal thrombus, since the largest diameter considered here is D = 4 cm, which is just below the critical size, above which an endoluminal thrombus has been clinically observed to develop (Harter *et al.* 1982).

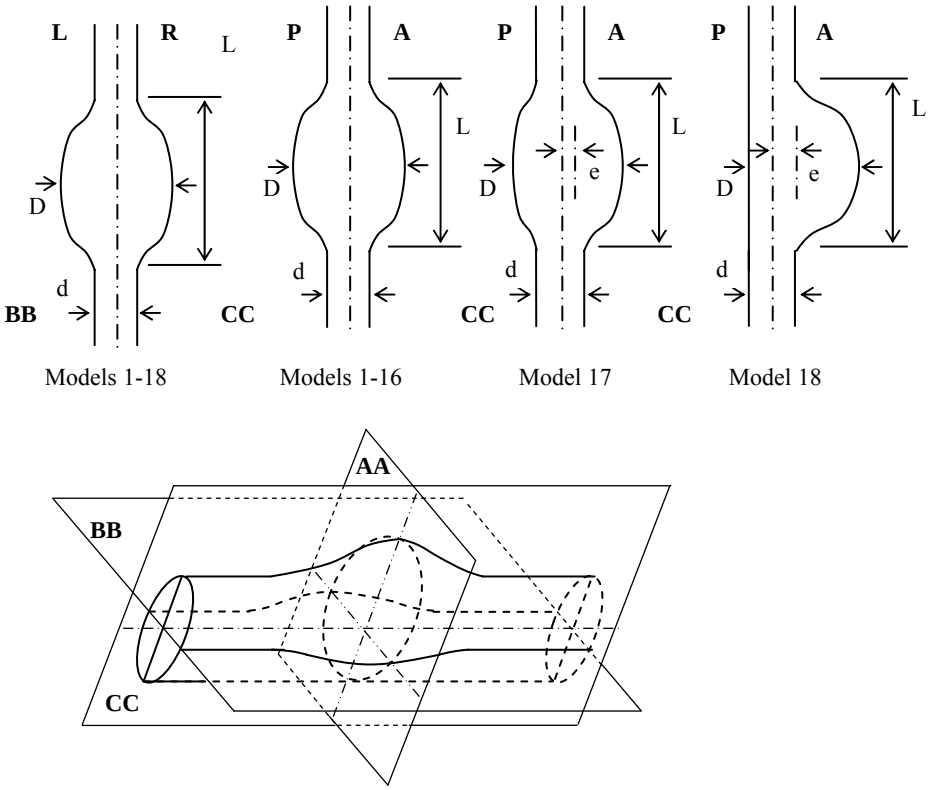

Figure 2.3: Geometry of the aneurysm models. L: left, R: right, P: posterior, A: anterior.

The models are made out of glass and are therefore rigid. AAAs have been shown to become much stiffer as they expand, because of the degradation of the elastin fibers in the walls (see Chapter 1). Calcification of the walls further increases the wall stiffness over time. Physiologically, the compliance of the arteries is crucial for the shaping of the flow waveform. However, in the experiment, the pump reproduces directly the flow

waveform measured in the infrarenal abdominal aorta. Therefore, the rigidity of the models does not affect the actual waveform inside the aneurysm.

		L/d		
	Models	2.9	3.9	5.2
D/d	1.3	*1*	*6*	*11*
	1.5	*2*	*7*	*12*
	1.7	*3*	*8*	*13*
	1.9	*4*	*9*	*14*
	2.1	*5*	*10*	*15*

Models	*D/d*	*L/d*	β
16	2.3	4.5	0
17	2.3	4.5	0.5
18	2.3	4.5	1

Table 2.I: Geometric parameters of the different models considered in the study. The first table indicates the values of the dilatation and aspect ratios for the 15 symmetric models considered in the first part of the study. The targeted aspect ratios were respectively 3, 4 and 5, but due to the inherent difficulty of the process of fabrication of the glass models, the ratios came out slightly different. The second table shows the 3 models considered in the study of the loss of symmetry. Larger dilatation and aspect ratios have been chosen, since the non-symmetry develops at later stages of the disease.

2. Experimental setup

Figure 2.4 schematically shows the experimental flow facility. The pulsatile flow is provided by a programmable piston pump (Sidac Engineering, Ontario, Canada). A micro-stepping motor (Compumotor Corporation, Cupertino, CA) controls the displacement of the piston on a rack inside a cylinder. The piston diameter is 6.3 cm and the cylinder contains a volume of 450 ml. Each time the piston reaches the end of the cylinder, a four-way spool valve (Numatics, Highlands, MI) reverses the inlet and outlet pathways, in order to always keep the flow in the same direction in the test section.

The programmable piston pump reproduces the abdominal aortic flow. The chosen waveform is based on the measurements by Maier *et al.* (1989), conducted in a healthy

male patient at rest (Figure 2.5). Similarly to the results by Long *et al.* (2000), it comprises a quite large reversal of the flow in the diastole, which has been shown to be the case in a healthy person at rest by Holenstein & Ku (1988). Retrograde flow at this point of the cycle is thought to provide blood flow to the coronary arteries (McDonald 1974; Caro *et al.* 1978). Other groups have, however, measured the abdominal aortic flow to have a very small reversal flow (Mills *et al.* 1970, Pedersen *et al.* 1993). For this study, we have elected the extreme case of a subsequent diastolic flow reversal. This choice should not affect greatly the key phenomena, which are the flow separation and the formation of a vortex. Flow separation is guaranteed to occur at the peak systole at the latest. Earlier flow separation will depend on the acceleration and on the geometric parameters of the model.

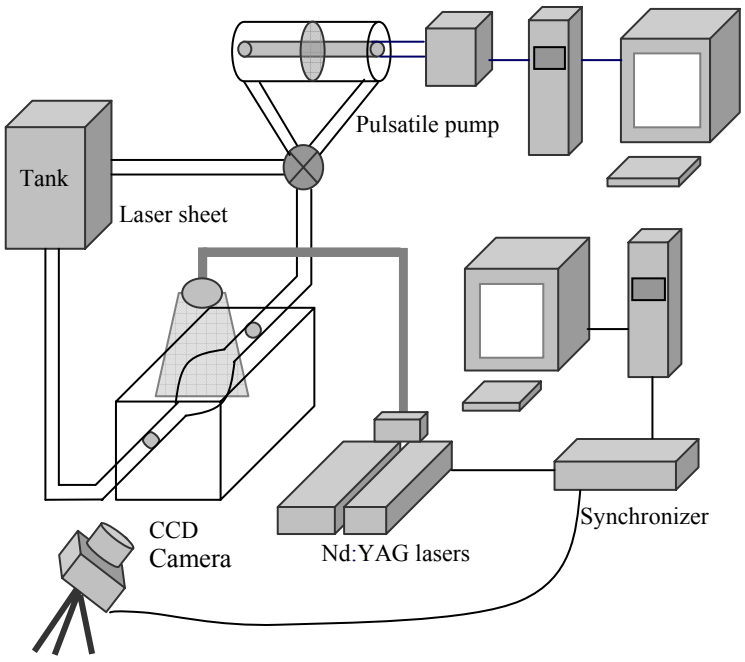

Figure 2.4: Experimental setup

By using water as the perfusion fluid, we neglected the non-Newtonian behavior of blood in the experiments. In the case of non-Newtonian fluids, the viscosity coefficient can still be assumed constant in the high shear stress regions, but it is a function of the stress in the regions of low shear stress. For large vessels, larger than 1 mm in diameter (Nichols 1998), the regions of low shear stresses are confined to the core of the fluid. Most of this study focuses on the quantification of the shear stresses at the wall, where they are the highest. The quantification of the shear stresses on individual blood cells may need a small correction factor for the few cells launched in the core of the aneurysm. Nevertheless, we will see that these cells either leave the aneurysm very quickly without noticing the presence of the aneurysm or they are entrained into the recirculating region, where they are again in closer contact with the wall. Assuming blood as Newtonian should therefore be a valid hypothesis.

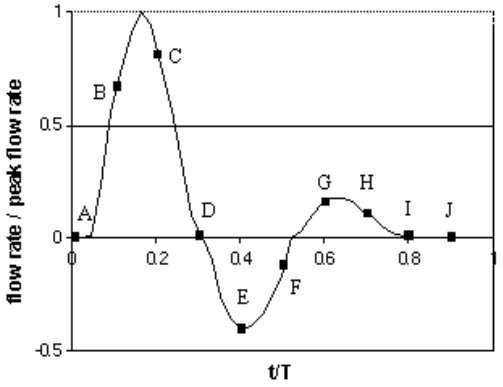

Figure 2.5: The waveform delivered by the pulsatile pump reproduces the typical infra-renal flow rate of a male patient at rest. The letters indicate the approximate times along the cardiac cycle when the measurements were made.

The use of pure water was dictated by the pump, which is not powerful enough to deliver the aortic sub-renal flow rate. The fluid viscosity was then reduced by a factor of 3.9, as compared to whole blood. In order to maintain a complete similarity, the aneurysm models were scaled down by a factor of 1.9 (d = 9 mm in the experiment). The goal was to keep both the Reynolds number, ratio of the convective inertial forces to the

viscous forces, and the Womersley number, ratio of the unsteady inertial forces to the viscous forces, identical to the physiological flow conditions. This complete similarity ensures that the Strouhal number remains constant as well, since it is proportional to $\alpha^2/\overline{Re}$, where $\alpha = d/2\sqrt{\omega/\nu}$, $\overline{Re} = \overline{U}d/\nu$, $\overline{U}$ being a characteristic cross-averaged velocity, ω the pulsation frequency of the flow and ν the fluid kinematic viscosity. More specifically, the flow conditions used in this study correspond to a peak Reynolds number of 2700, a mean Reynolds number of 330 and a Womersley number of 10.7. With a same peak Reynolds number, the mean Reynolds number would have been higher if we had chosen to use a flow waveform without flow reversal ($\langle \overline{Re} \rangle \sim 550$). The measured quantities (velocity, vorticity, stresses) presented in the next sections have been converted into the physiological values.

B. Particle Image Velocimetry

Particle Image Velocimetry (PIV) measurements of the instantaneous velocity field have been conducted in a cross-section of the AAA. The PIV system (TSI Incorporated, St Paul, MN) is composed of two 50 mJ pulsed Nd:YAG lasers, a synchronizer and a CCD camera (Figure 2.4). The lasers produce short duration (6 ns), high-energy (12 mJ) pulses of light in the green band (532 nm). The energy is produced from a flashlight that can be fired at variable frequencies up to 10 Hz. The use of two lasers allows us to control very precisely the time between two pulses. Any pulse separation can be achieved from very short to long, while maintaining the full power in each laser. The light beam is converted into a light sheet using consecutively a cylindrical and a spherical lens. The laser sheet is 1 mm thick at the focal point.

Optical access to the model is provided at two orthogonal locations, one for the laser sheet and the other for the CCD camera (630046 PIVCAM 10-30), which has a resolution of 1024×1024 pixels and a 8-bit dynamic range. The flow is seeded with 10 μm-diameter

lypocodium particles (Carolina Biological Supply Company, Burlington, NC), which are illuminated each time the lasers are fired. The AAA models are placed in a transparent box filled with water in order to limit optical deformations due to refractions. The light scattered by the tracer particles are recorded by the camera, which is synchronized with the lasers (TSI Laserpulse^{TM} synchronizer). The displacements of the particles are obtained by locally cross-correlating sequential images recorded by the camera. The cross-correlation function for an image pair is calculated using fast Fourier transforms. The interrogation window is 64×64 pixels in size and a 50% overlapping is employed in both directions. The resolution varies from one experiment to the next, depending on the total size of the measurement window. It ranges between 0.4 mm for the zoom measurements to 1.8 mm for the larger aneurysm models. The few incorrect vectors have then been removed by hand and replaced with an interpolated vector. No post-processing smoothing or averaging function has been used. The velocity vectors are computed knowing the time interval between two pulses of the lasers. Validation of the measured velocity field will be discussed in Chapter 3, when comparing the measurements in a healthy vessel with the Womersley solution.